Thermal, mechanical and microstructural characterization and antioxidant potential of Rhinobatos cemiculus gelatin films supplemented by titanium dioxide doped silver nanoparticles

Soumaya Boughriba, Nabil Souissi, Mourad Jridi, S.M. Li, Moncef Nasri

Thermal, mechanical and microstructural characterization and antioxidant potential of *Rhinobatos cemiculus* gelatin films supplemented by titanium dioxide doped silver nanoparticles

Soumaya Boughriba[† a,b], Nabil Souissi [c], Mourad Jridi [a], Suming Li [b] and Moncef Nasri [a]

[a] *Laboratoire de Génie Enzymatique et de Microbiologie, Université de Sfax, Ecole Nationale d'Ingénieurs de Sfax, B.P. 1173-3038 Sfax, Tunisia.*

[b] *Institut européen des membranes, UMR CNRS 5635, Université de Montpellier, Place Eugene Bataillon, 34095 Montpellier Cedex 5, France.*

[c] *Laboratoire de Biodiversité Marine, Institut National des Sciences et Technologies de la Mer, Centre de Sfax, Avenue Madagascar BP, 1035-3018, Sfax, Tunisia.*

† Corresponding author. Tel.: +216 99157657 ; Fax: +216 74275595.

Soumaya Boughriba: Laboratoire de Génie Enzymatique et de Microbiologie, Université de Sfax, Ecole Nationale d'Ingénieurs de Sfax, B.P. 1173-3038 Sfax, Tunisia.

E-mail address: soumaya.boughriba@gmail.com

Abstract

Hybrid composites films were prepared by the incorporation of titanium dioxide doped silver nanoparticles (TiO_2-Ag NPs) at different concentrations (1, 2, 3 and 4 wt%) into *Rhinobatos cemiculus* gelatin (RCG) matrix. The microstructure analysis, realized by scanning electron microscopy and atomic force microscopy revealed a homogenous structure and a smooth surface of the composite films. The mechanical properties, light transmission and moisture content of composite films are greatly dependent on the amount of added TiO_2-Ag NPs. A gradual decrease in elongation at break was observed with the increase in TiO_2-Ag nanoparticles content (reaching 16.05% at an addition level of 4%). Moreover, the addition of TiO_2-Ag NPs considerably enhanced the antioxidant activity of nanocomposite films evaluated by DPPH radical scavenging activity and ferrous chelating activity. It is, thus, concluded that the incorporation of TiO_2-Ag NPs into the gelatin matrix promotes the improvement of gelatin films' performance.

Keywords: *Rhinobatos cemiculus*, gelatin, nanoparticles, nanocomposite films, thermal analysis, microstructural and mechanical properties.

Introduction

Biopolymers are considered as a promising alternative to petrochemical based polymers for the sake of environment protection and sustainable development (Félix, Lucio-Villegas, Romero, & Guerrero, 2016). Several market studies showed that with feedstock's low cost and technologies, the biopolymer demand exceeds an annual growth rate of 4.5 times of the current production between 2014 and 2019 (Galiano, et al., 2018). Moreover, consumers are also more and more interested in products based on biopolymers regarding their low toxicity, biodegradability and biocompatibility (Galiano, et al., 2018).

Currently, the fish processing industries as well as the fish markets are providing large amounts of by-products and wastes serving as raw materials for the extraction of various biopolymers. Among these wastes, skin (Arumugam, Sharma, Balakrishnan, & Ettiyappan, 2018), bones (Maccari, Galeotti, & Volpi, 2015), exoskeletons (Hamdi, et al., 2017) and viscera (Abdelhedi, Nasri, Souissi, Nasri, & Jridi, 2016) are the most exploited. The skin gelatin from multiple fish species such as *Nile tilapia* (Zheng, et al., 2018), *Hemiramphus far* (Abdelhedi, et al., 2019), *Cyprinus carpio* (Tkaczewska, Morawska, Kulawik, & Zając, 2018), *Loligo formosana* (Hamzeh, Benjakul, Sae-leaw, & Sinthusamran, 2018) and *Probarbus jullieni* (Ali, Kishimura, & Benjakul, 2018) has been extracted and characterized. Gelatin is a protein produced by thermal denaturation of collagen. It is widely used in food industries as a thickening agent in desserts, a stabilizer in ice cream preparations, a texturizer in confections' production, and as food foam and gelling agent (Handbook, 2012; Haug, Draget, & Smidsrød, 2004; Karayannakidis & Zotos, 2016; Karim & Bhat, 2008; Schrieber & Gareis, 2007). In addition, the intrinsic properties of gelatin, especially its excellent film forming ability (Arfat, Benjakul, Prodpran, & Osako, 2014) nowadays offer substantial advantages for uses in membrane technology. In fact, gelatin-based membranes showed a growing interest in water treatment (Kamal, Pochat-Bohatier, & Sanchez-Marcano, 2017), gas

separation, micro and ultra-separation as well as for tissue engineering (Tayebi, Rasoulianboroujeni, Cui, & Ye, 2018) where they are used not only as barriers to volatile compounds, oxygen and carbon dioxide, but also as carriers of a wide variety of substances, such as antioxidants, antibacterial agents, colorants, and nutrients (Ahmad, Benjakul, Prodpran, & Agustini, 2012).

Nevertheless, gelatin membranes exhibit poor mechanical and thermal properties, which restrict their use as a packaging material (Gómez-Guillén, et al., 2009). Using nanoparticles in biopolymer-based films is a promising alternative to improve both mechanical and thermal properties (Shankar & Rhim, 2018). Among these nanoparticles, titanium dioxide and silver nanoparticles (TiO_2-NP and Ag-NP) are the most commonly manufactured (Chen, et al., 2016). In fact, TiO_2-NPs are gaining special attention thanks to their low cost, high stability, photo-catalytic and anticorrosive properties (Feng, et al., 2007). A recent study has shown that TiO_2-NPs could avoid light induced oxidation and decomposition when used in food packaging systems (Vejdan, Ojagh, Adeli, & Abdollahi, 2016). In addition, these NPs have been used as an UV protective skin compound as they have wide UV spectrum-attenuation characteristics (Schulz, et al., 2002). On the other hand, silver nanoparticles displayed an inhibitory and bactericidal effect thanks to their high surface area (Mangalaraj & Devi, 2017; Yan, et al., 2007). They are considered as a non-specific bactericide agent able to act against a broad spectrum of bacterial and fungal species (Raghunath & Perumal, 2017). A supplementary layer, of titanium dioxide as an example, is often added to prevent silver oxidation and reduce its concentration (Mangalaraj, et al., 2017).

In this respect, this work aimed to develop novel films based on *R. cemiculus* gelatin supplemented with TiO_2-Ag nanoparticles. The physicochemical, thermal, mechanical and antioxidant properties of the prepared films were then investigated.

2. Materials and methods

2.1. Gelatin extraction

Fresh blackchin guitarfish (*R. cemiculus*) skin was supplied from the local fish market located in Sfax, Tunisia. Samples were placed in ice and then transported in polyethylene bags to the laboratory. The skin was rigorously washed and stored at -20 °C before gelatin extraction.

Gelatin was extracted according to the protocol described by Jridi, et al. (2013) with slight modifications. Once thawed, the blackchin guitarfish skin was cut into small pieces with an electric carving knife, and then soaked in 0.05 M NaOH (1:5, w/v) under continuous stirring for 2 h at 25 °C. The medium was changed every 30 min to ensure better elimination of non-collagenous species. Thereafter, the alkaline treated skin pieces were washed with distilled water until a neutral pH value of the washing solution was reached. They were then soaked in 0.2 M acetic acid solution (ratio 1:5, w/v) for 18 h at 25 °C. Thereafter, the pH of the medium was adjusted to 7.0 using NaOH solution. The gelatin extraction was realized at 50 °C for 18 h under continuous stirring. The centrifugation was carried out at 8 000 g for 30 min at 4 °C to remove insoluble residues. Finally, the supernatant was collected and freeze-dried (Moduloyd freeze dryer thermo fisher, USA) to obtain *R. cemiculus* gelatin (RCG) powder.

2.2. Electrophoretic analysis

The protein patterns of the extracted gelatin were determined using the sodium dodecyl sulphate–polyacrylamide gel electrophoresis (SDS–PAGE) as described by Laemmli (1970) with slight modifications. The gelatin (10 mg) was dissolved in 1 ml of distilled water at 50 °C. 50 µg of each sample were mixed with loading buffer (5% mercaptoethanol, 2% SDS and 0.002% bromophenol blue) at a ratio of 1:5. The prepared mixtures were heated at 90 °C for 10 min and then loaded onto 5% w/v stacking gel and 7.5% w/v separating gel.

126 **2.3. Turbidity determination**

127 The gelatin turbidity was evaluated using the method described by Fernández-Díaz,
128 Montero, & Gómez-Guillén (2001). Briefly, the absorbance at 360 nm was measured after
129 dissolving the dry gelatin powder in distilled water at a concentration of 6.67% (w/v). Then an
130 adjustment of the pH ranging from 2 to 10, using either 10 mM HCl or 10 mM NaOH, was
131 carried out. Experiments for each sample were fulfilled in triplicate (Fernández-Díaz,
132 Montero, & Gómez-Guillén, 2001).

133 **2.4. Films' preparation**

134 The gelatin/titanium dioxide-silver films were developed through a simple casting
135 approach. Nanoparticles with size ranging within 15 – 20 nm, were obtained as described by
136 Elleuch, et al. (2020). First, the RCG powder (4 g) was solubilized in 100 ml of distilled water
137 under magnetic stirring at 50 °C. The titanium dioxide doped silver nanoparticles (TiO_2-Ag)
138 were added at different ratios to the solution (1, 2, 3 and 4 wt %). Glycerol was then added to
139 the mixture as a plasticizer at a concentration of 15 % (w/w, plasticizer/polymer dry matter),
140 and the mixture was stirred for 30 min. The sonication was subsequently applied using an
141 Elmasonic S10 H ultrasound cleaner in order to guarantee a homogeneous dispersion of
142 nanoparticles in the mixture. 25 ml of each solution was then poured into a Petri dish of 13.5
143 cm diameter, and allowed to dry under an air flow of a laboratory hood at 25 °C for 48 h.
144 Finally, the films were peeled off and preserved at 25 °C before use.

145 **2.5. Moisture content**

146 The moisture content (MC) of each sample was determined by drying 100 mg of film
147 specimens in an oven (Memmert UF1060) at 105 °C for 24 h. The MC values, evaluated in
148 triplicate, were obtained by weighing samples before and after oven drying. The results were
149 expressed as g moisture/100 g film.

150

151

152 **2.6. Water solubility**

153 The films' water solubility (WS) was carried out via the method described by
154 Gennadios, Handa, Froning, Weller, and Hanna (1998). Samples (100 mg) were weighed and
155 then placed in a centrifuge tube containing 30 ml of distilled water. The tubes were then
156 shaken at 25 °C for 24 h, and then centrifuged at 10000 g for 10 min at 25 °C (Labogene,
157 ScanSpeed 1248R centrifuge). The supernatant was discarded, and the pellet corresponding to
158 the non-solubilized film was dried at 105 °C for 24 h. The water solubility was carried out in
159 triplicate and expressed as follows:

$$WS\ (\%) = \frac{(m_i \times (100 - M_C) - m_f) \times 100}{m_i \times (100 - M_C)}$$

160 where m_i is the initial film mass (g), m_f the final dry film mass (g), M_C the moisture content
161 (%).

162 **2.7. Color parameters**

163 The color of RCG-TiO_2-Ag NPs films was evaluated using a bench-top colorimeter
164 (CR-5; Konica Minolta). The values were expressed by referring to a white standard color
165 plate used as a background. The color parameters, L^*, a^* and b^* expressing
166 lightness/brightness, redness/greenness and yellowness/blueness, respectively, were
167 determined. The difference in color ΔE was determined as described by Sinthusamran,
168 Benjakul, Hemar and Kishimura, (2018).

$$\Delta E = \sqrt{(\Delta L)^2 + (\Delta a)^2 + (\Delta b)^2}$$

169 **2.8. Ultraviolet-visible absorption spectrum**

170 The difference in gelatin films' absorption as a function of the nanoparticles' content
171 was determined in a wavelength ranged from 200 to 800 nm using a spectrophotometer

(JENWAY, 7315 spectrophotometer), as described by Nagarajan, Benjakul, Prodpran, and Songtipya (2012).

2.9. Fourier transform infrared spectroscopy

The Fourier transform infrared spectroscopy (FTIR) spectra were obtained using Thermo Fisher Scientific spectrometer (Model: Nexus). The sample compartment was equipped with an attenuated total reflectance (ATR) accessory. The reflection incidence angle of the diamond crystal was about 45° with respect to the IR beam. A resolution of 4 cm^{-1} and a number of 32 scans were used to obtain the spectra in the 4000-600 cm^{-1} range at room temperature.

2.10. X-ray diffraction analysis

The X-ray diffraction (XRD) patterns were collected on Bruker D5000 ray diffractometer using a Cu Kα radiation source. The analyses were operated at 40 kW and 20 mA and the patterns were recorded in the range of 2Θ= 7-40° at a scanning rate of 1°/min.

2.11. Thermal analysis

The differential scanning calorimetry (DSC) was carried out using DSC Q20, TA Instrument in order to determine the thermal properties of different prepared films. Samples (5 mg each) were subjected to two cycles of heating-cooling from -50 °C to 200 °C with a heating rate of 10 °C/min. The nitrogen purge was applied at a flow rate of 50 ml/min. The obtained DSC thermograms were treated using TA Universal Analysis 2000 software (version 4.5 A, TA instruments). The glass transition temperature (Tg) was determined as the mid-point of the second heating cycle. In order to determine thermal stability, thermogravimetric analysis (TGA) was performed using TGA Q500 High Resolution, TA Instruments. Samples (5 mg each) were heated from 25 to 800 °C at a heating rate of 20 °C/min under air flow. The thermograms were obtained using TA Universal Analysis 2000 software (version 4.5 A).

2.12. Mechanical properties

The mechanical properties of RCG-films were measured in terms of tensile strength (TS) and elongation at break (EAB) using a rheometer apparatus (Physica MCR 301, Anton Paar, GmbH, France) equipped with a measuring geometry (CTD 450). Rectangular samples of 1.0 cm x 4.5 cm were prepared for measurements. Prior to testing, all samples were conditioned at 25 °C and 50 % relative humidity for two weeks, and the thickness was measured. The film samples were fixed on the extension grips, and then deformed uniaxially under a deformation rate of 5 mm/min until breaking, based on the ISO standard conditions. The stress-strain curves were attained using the Rheoplus software. The maximum TS and the final EAB were determined. Values between 4 to 6 measurements were saved and used for calculations.

2.13. Microstructure and surface topography analysis

The microstructure of RCG-TiO_2-Ag NPs films was examined using Hitachi S4800 scanning electron microscope (SEM). Prior to analysis, the samples were sputtered with a thin gold layer of 5 nm. An accelerating voltage of 2.0 kV was applied to observe the surface and the cross-section morphology of the film samples. The surface topography of the film samples was further examined using a dimension 3100 atomic force microscopy (AFM) apparatus (Digital Instruments, Veeco, CA). The experiments were conducted at ambient temperature in an intermittent tapping mode. Data were processed using Gwyddion software (version 2.14).

2.14. Antioxidant activities

2.14.1. DPPH radical-scavenging activity

The DPPH radical scavenging activity of the gelatin films was determined according to the method described by Bersuder, Hole, and Smith (1998). The absorbance was determined at 517 nm. The DPPH radical scavenging activity was calculated as expressed in the following formula:

$$\text{DPPH radical} - \text{scavenging activity (\%)} = \frac{OD_{control} + OD_{blank} - OD_{sample}}{OD_{control}} \times 100$$

where OD_{blank}, $OD_{control}$ and OD_{sample} are the absorbance of the blank, DPPH control and sample reaction, respectively. The experiments were carried out in triplicate.

2.14.2. Ferrous chelating activity

The chelating effect of the gelatin films was determined according to the method of E. A. Decker and Welch (1990) with slight modifications. The method is based on inhibiting the formation of Fe^{2+}-Ferrozine complex in presence of the studied sample. Initially, 100 mg of each film was mixed with 100 µl of distilled water to which 50 µl of 2 mM $FeCl_2$ and 450 µl of distilled water were added. After 5 min of incubation, 200 µl of ferrozine solution (5 mM) were added, and the mixture was incubated again for 10 min at room temperature. Ethylene-diamine-tetra-acetic acid (EDTA) was employed as a positive control. The absorbance was determined at 562 nm for each sample. The ferrous chelating activity was calculated as expressed in the following formula:

$$\text{Metal chelating activity (\%)} = \frac{OD_{control} + OD_{blank} - OD_{sample}}{OD_{control}} \times 100$$

where $OD_{control}$, OD_{blank}, and OD_{sample} are the absorbances of the control, blank and sample reactions, respectively.

2.15. Statistical analysis

The statistical analyses were performed with SPSS version 17.0, professional edition using ANOVA analysis. A standard deviation at a confidence level of 95% was used to compare all parameters analyzed for all elaborated films.

3. Results and discussion

3.1. Electrophoretic analysis for RCG

The molecular weight distribution of RCG was analyzed by SDS-PAGE (Fig. 1). The resulting pattern showed the presence of all gelatin characteristic chains, specifically β and

α_1/α_2 with MW of 200 and 120-130 kDa, respectively, as previously reported by Gomez Guillen et al. (2009) and Tümerkan, Cansu, Boran, Mac Regenstein, and Özoğul (2019). In fact, α_1 and α_2 chains intensities for *R. cemiculus* skin gelatin were almost similar. Additionally, high molecular-weight components resulting from residual heat-stable cross-links were found in RCG, as proved by the high-intensity band at the top of the polyacrylamide gel. On the other hand, owing to the higher molecular weight of β-chain, dimer of α -chain, it might not be extracted effectively as demonstrated by the lower band intensity in the obtained gelatin. Nagarajan et al. (2012) demonstrated that a higher content in α-chain reflected better functional properties for splendid squid skin gelatin. Liu, Li, and Guo (2008) confirmed that β- and γ- chains would permit a more organized structure with a higher gel strength. Large amounts of β- and γ-chains have been shown to negatively affect some of the functional properties of fish gelatins, such as lower viscosity and melting point (Muyonga, Cole, & Duodu, 2004).

3.2. Turbidity analysis

The gelatin solution turbidity was evaluated by measuring the absorbance measurement at 360 nm and results were illustrated in Fig. 2. The results showed that the highest turbidity of RCG was obtained at pH 5. For higher and lower pH values, turbidity values decreased. Similarly, Lassoued, et al. (2014) reported that the turbidity was influenced by pH variation. Poppe (1997) reported that the gelatin solutions showed the maximum of turbidity at their isoelectric point. This could be explained by the fact that at pH close to pI, the protein molecules lean to form aggregate and less water interaction might take place with the protein molecules.

3.3. Film solubility

Solubility is an essential property of edible films since they are used as protective coatings on food. Potential applications may necessitate water insolubility to enhance product

integrity and water resistance (De Moura, Lorevice, Mattoso, & Zucolotto, 2011). For this purpose, the RCG films' solubility was determined and the values are represented in Table 1. Native gelatin films exhibit almost 33 % of solubility in pure water due to its hydrophilic nature caused by the presence of polar peptides in gelatin. With the addition of TiO_2-Ag NPs to the film matrix, a decrease in the solubility was detected, which could be attributed to the formation of hydrogen bonds between the gelatin matrix and the nanoparticles resulting in a reduction of interactions between the biopolymer and water molecules, causing solubility decrease (Voon, Bhat, Easa, Liong, & Karim, 2012). Similar findings were obtained in previous studies where gelatin films were added with SiO_2 nanoparticles and showed a decrease in water solubility. Additionally, for other biopolymer-based films, a decrease in water solubility has been perceived once the nanoparticles, such as chitosan nanoparticles in hydroxypropyl methylcellulose films (M. De Moura, Avena‐Bustillos, McHugh, Krochta, & Mattoso, 2008) and sodium montmorillonite in methyl cellulose films (Tunç & Duman, 2010), were added.

3.4. Color

Color is an important parameter that should be controlled as it affects consumers' acceptance (Pereda, Dufresne, Aranguren, & Marcovich, 2014). Color parameters in terms of rectangular coordinates (a^*, $b^*$and L^*) and total color difference (ΔE) of the various films are presented in Table 2. With the addition of TiO_2-Ag NPs, the values of a^* and b^* increased while the L^* value decreased, indicating the leaning toward red and yellow colors. In fact, the RCG films supplemented with 4% of TiO_2-Ag NPs presented the highest a^*, b^* and ΔE values of 0.76±0.11, 4.16±0.37 and 14.85±1.0, respectively and the lowest value of L^* of about 94.09±0.57. The reduced L* value demonstrated that the films became darker with the addition of TiO_2-Ag NPs, which is in accordance with the visual observations. These changes in color were most likely attributed to TiO_2-Ag NPs color which is initially brownish-gray as

described by Naoi, Ohko, and Tatsuma (2005). Therefore, if the composite is intended to be employed as edible coating material, the percentage of TiO_2-Ag NPs has to be carefully controlled to keep the initial color of the coated product, as mentioned by Jamróz, Kulawik, and Kopel (2019).

3.5. Light transmittance

The transmission of UV and visible light of the films in the wavelength ranged from 200 to 800 nm is illustrated in Fig. 3. The UV light transmission for all films was low at 200-280 nm. These results may be due to the presence of chromophore groups in aromatic amino acids constituting the gelatin matrix such as tyrosine and phenylalanine, which have strong absorption of UV light (Gómez-Guillén, et al., 2009; Kchaou, et al., 2017; Nagarajan, et al., 2012). Figure 3 also shows that the light transmission of the films rapidly increased in the range from 280 to 400 nm, and then leveled off in the visible range. It is also noted that the light transmission decreased with the increase of nanoparticles content, suggesting that TiO_2-Ag NPs were well integrated into the gelatin matrix. Therefore, their UV light transmission was reduced.

3.6. FTIR analysis of RCG based nanocomposite films

FTIR was used to investigate the molecular interaction in RCG films incorporated with different amounts of TiO_2-Ag NPs. The FTIR spectra of all prepared gelatin films in the spectral ranged between 600 and 4000 cm^{-1} are shown in Fig. 4. Generally, the prepared films showed similar spectra in the range of 600-1800 cm^{-1}, presenting amide I, amide II and amide III bands as found by Arfat, et al. (2016). The most pronounced absorptions appeared at wavenumbers ranging between 1560-1680 cm^{-1}, 1540-1610 cm^{-1} and 1230-1340 cm^{-1}, which are attributed to typical absorptions normally detected for gelatin-based films as amide I (C=O stretching at $\sim 1630\ cm^{-1}$), amide II (N-H groups coupled with C-N stretching at $\sim 1540\ cm^{-1}$) and amide III (C-N and N-H stretch and vibrations of CH_2 groups of glycine),

respectively (Nur Hanani, Beatty, Roos, Morris, & Kerry, 2013; Tongnuanchan, Benjakul, & Prodpran, 2012). Peaks related to amide A were detected at 3300-3500 cm^{-1} as described by Fundo, Galvis-Sanchez, Delgadillo, Silva, and Quintas (2015). The peak detected at 1080 cm^{-1} referred to the C-O of the glycerol (Bergo, Moraes, & Sobral, 2013), used as a plasticizer. These results showed that no notable changes in the shifting or density of peaks related to gelatin occurred regardless of TiO_2-Ag NPs addition, except for the O-H stretch indicating the arrangement of intermolecular hydrogen bonds (Qiao, et al., 2017).

3.7. X-ray diffraction (XRD) analysis

The XRD patterns of gelatin films with various TiO2-Ag NPs contents are shown in Fig. 5. An amorphous halo is observed for all the films. In contrast, the composites with 2, 3 and 4% TiO_2-Ag NPs displayed a crystalline peak at $2\theta = 25.8$ characteristic of the diffraction of TiO_2 crystal (Ba-Abbad, Kadhum, Mohamad, Takriff, & Sopian, 2012). No peak was detected for the Ag crystal, indicating that the silver core was amorphous and that the nanoparticles used were effectively composed of a non-oxidized silver core protected by the TiO_2 layer. These results are in accordance with those reported by Li, Xu, Chen, and Chen (2011) who suggested that at low contents of nanoparticles, the protein adsorption on the surface of particles reduced their crystallization which became undetectable in the XRD. Meanwhile, self-assembled nanoparticle agglomerates taking place at high concentration of nanoparticles (2 g/100 g) could regain their crystallization capacity.

3.8. Gelatin thermal properties

3.8.1. Determination of gelatin glass transition temperature

The thermal properties of gelatin sample were characterized using DSC to determine the corresponding glass transition temperature (Tg). It's demonstrated through the DSC curves (data not shown) that a glass transition temperature of almost 150 °C was obtained for the extracted gelatin. The obtained value was higher than the Tg values of commercial bovine

(74.8 ºC) and fish (68.1 ºC) gelatins (Al-Hassan, 2020). The glass transition temperature is defined as the temperature at which the polymer relaxes and changes form the glassy state to the elastic state, for a given heating rate due to the onset of long-range coordinated molecular motion of the amorphous structure (Sperling, 2005). The difference between RCG and the cited commercial bovine and fish gelatins Tg values could be related to its structural characteristics that might change as a function of molecular mobility (Rahman, Al-Saidi, & Guizani, 2008). The rigidity and mobility of the polymer particularly play a crucial role in the improvement of the glass-forming ability (Minecka, et al., 2020). In addition, Bell & Touma (1996) explicated that the variation of Tg may be due to different types of gelatin transformed through different extraction methods. Besides, it could also be related to characteristics of animals' skins based on species and age.

3.8.2. Evaluation of gelatin thermal stability

The TGA curves of the extracted gelatin are presented in Fig. 6a. The studied gelatin powder shows a minor loss in weight below 100 °C, corresponding to moisture release. A major weight loss was detected from 250 to 450 °C, corresponding to the thermal decomposition of gelatin. Chuaynukul, Prodpran, and Benjakul (2014) suggested that the water adsorbed influenced the protein-protein interaction by reducing the thermal stability of the gelatin system. A high content in water leads to a possible protein degradation that is more likely to take place in a greater degree especially at high temperature. Thus, a greater loss of thermal stability of protein is attained.

3.9. Nanocomposite films thermal properties

The differential scanning calorimetric (DSC) analysis was carried out to determine the thermal properties of nanocomposites. The results of Table 1 summarized the values of the glass transition (Tg) of RCG-Ag-TiO_2 films. The RCG control film exhibited a Tg value of about 59.52 °C which is higher than those found by Hazirah, Isa, and Sarbon (2016) and

Theerawitayaart, Prodpran, Benjakul, and Sookchoo (2019) estimated at 48.4 and 56.4 °C, respectively. The Tg of composite films decreased with the increase of TiO_2-Ag NPs content, reaching 52.61°C for 4% of NPs. This decrease may be attributed to a disorder state among gelatin molecules or the net-like structure of the gelatin molecules according to the theory related to molecular interactions and chain stiffness previously described by Luecha, Sozer, and Kokini (2010) with corn zein/montmorillonite gelatin. Moreover, the Tg decrease may also be caused by the hydrophobic feature due to TiO_2-Ag nanoparticles added in the gelatin matrix (Bahadur & Uludağ, 2016). This phenomenon facilitated water evaporation and consequently decreased hydrogen bonding as described by Wu, Liu, Wang, Han, and Liu (2017). Furthermore, lower Tg values were probably related to the decrease in hydrogen bonds initially existing in the gelatin based film (Chak, Kumar, & Visht, 2013).

The thermal stability of composite films was evaluated using TGA and DTG. As shown in Fig. 6c, the RCG control film and that added with 1% of TiO_2-Ag NPs exhibited a five-step weight loss pattern, whereas other composite films showed 3 decomposition phases. As shown in Fig. 6c, the first phase started around 60 °C for control RCG film and between 80 and 100 °C for the composites owing to the evaporation of free and bound water remaining in the films (Rhim, Hong, Park, & Ng, 2006). As the temperature increased from 120 to 800 °C, a peak at 250 °C appeared in all thermograms due to the blending of glycerol as a plasticizer in all prepared gelatin films. The third weight loss, which exhibits a strong exothermic peak at 320–350 °C for all films, was due to the decomposition of lower molecular weight gelatin fractions (Arfat, et al., 2016). The peak at 500 °C, which almost disappeared for films prepared with 2, 3 and 4% of TiO2-Ag NPs, was related to the degradation of highly interacted proteins in the gelatin matrix (Arfat, et al., 2016). The absence of this decomposition step for the composites with TiO_2-Ag NPs contents above 2% proved the enhancement of the thermal stability of these films at 500 °C, mostly due to the heat-stable TiO_2-Ag NPs, in agreement with data

reported by Rhim, et al. (2006) for gelatin-silver nanoparticle added-composite films. The last degradation stage occurs between 550 and 700 °C for films added with 0%, 1% and 4% and corresponds to the thermal decomposition of the gelatin networks (Mishra, Majeed, & Banthia, 2011). These results proved that RCG films added with 2 and 3% are thermally stable until approximately 800 °C.

3.10. Mechanical properties of RCG/TiO_2-Ag NPs composite films

Gelatin films are widely used in various industrial packaging processes. Thus, their resistance to stretching is of major importance for their applications. The effect of TiO_2-Ag nanoparticles' addition on the mechanical properties of RCG-films was investigated in terms of TS and EAB as summarized in Table 1. The control film exhibited the highest EAB (28.1±2.5%) compared to nanoparticles-added films. In fact, the EAB decreased from 21.6±0.3 to 16.1±1.8% with increasing NPs content from 1 to 4%. Some reported differences might be due to the source from which the gelatin was extracted, the composition, the type and ratio of the added plasticizer as well as the preparation and storage methods. Moreover, the moisture content of the native gelatin film (49 g moisture/100 g wet basis film) decreased after the addition of nanoparticles to reach 26.5, 28.4, 27.8 and 31.3 for films added with 1, 2, 3 and 4%, respectively. Serrano-León, et al. (2018) proved that a decrease in moisture content values leads to a decrease in the molecular motion. Thus, mechanical properties of the prepared films could be affected by water content as well as nanoparticles addition. Data in Table 1 also show that the TS of the films decreased with the increase of TiO_2-Ag NPs. Compared to the value of 7.1 MPa for the control film, the TS decreased to 5.9, 5.4, 5.3 and 5.2 MPa for composites with 1, 2, 3 and 4% of TiO_2-Ag NPs, respectively. This decrease could be related to the configuration of the film's macromolecular network. In fact, the decrease of the mechanical characteristics of the nanocomposite films could be due to the heterogeneous distribution of TiO2-Ag NPs resulting in the slight aggregation occurring once

the concentration of nanoparticles is increased in protein matrix. The aggregate could inhibit the arrangement of protein domains and distant gelatin macromolecules will be found to construct the nanocomposite matrix resulting then in reduced mechanical properties of the prepared films. Hence, the concentration of TiO2-Ag nanoparticles was a main factor affecting both the spatial organization and the structure of protein aggregates in the film matrix. Similar findings were presented by Zhou, Wang, and Gunasekaran (2009) for whey protein/titanium oxide films and by Arfat, et al. (2016) for fish skin gelatin / fish protein isolate-zinc oxide nanocomposite films. Hence, the incorporation of TiO2-Ag NPs at a particular level could control the strength of the elaborated gelatin/ NPs films.

3.11. Microstructure of RCG/TiO_2-Ag NPs composite films

The surface and cross section microstructure of the composite films was examined with SEM as illustrated in Fig. 7. The surface of the control film (Fig. 7B) revealed a homogenous and smooth structure without cracks. Concerning the nanocomposite films, the NPs were dispersed uniformly, and the degree of dispersion increased as the content in nanoparticles increased (Fig. 7 B1-B4). Similar findings have been reported by Hosseini, Rezaei, Zandi, and Farahmandghavi (2015) where the chitosan nanoparticles were added to reinforce fish gelatin-based films. The cross section graphs were represented in Fig. 7 A1-A4 and revealed that the addition of Ti-Ag NPs caused changes in the microstructure of films, whereas the non-added film displayed a less undulated surface as supposed for homogeneous material. SEM micrographs of films containing 1%, 2% and 3% of Ti-Ag NPs showed an equi-distribution of particles in the gelatin matrix, without any observed aggregation. To further study the changes in TiO_2-Ag NPs aggregation and film roughness, three-dimensional (3D) images of the films' surface were obtained *via* AFM as illustrated in Fig. 8. The control RCG film was almost smooth. The addition of TiO_2-Ag NPs triggered a rougher surface for nanocomposite films due to the slight aggregation of nanoparticles. Moreover, the surface roughness was about 7.2

nm for the control RCG film, and increased from 10.5 to 18.2 nm when varying NPs content from 1 to 4%. This increase was assigned to the level of nanoparticles overlapping and the undulating surface of RCG film as described by Chang, Chen, Lin, and Chen (2012). Consequently, the excessive added TiO_2-Ag NPs amount of 4% is believed to incite the rift of the stable 3D polymeric matrix. Based on SEM and AFM results, it may be concluded that the nanocomposite films are relatively smooth thanks to the uniform distribution of the added nanoparticles and the tight combination with the gelatin matrix.

3.12. Antioxidant activity

The antioxidative potential of some substances could be acquired *via* various mechanisms. In fact, the antioxidant defense systems operate through obstructing the production of free radicals, obstructing the secondary production of inflammatory mediators, scavenging the oxidants, obstructing the chain propagation of these oxidants and improving the endogenous antioxidant defense system of the substance in question. These defense tools act together to defend the body from oxidative stress (H. Decker & Rimke, 1998). For this purpose, the DPPH radical scavenging activity and the metal chelating activity of the films were determined as shown in Fig. 9. The first one is based on free radicals capture, and the latter is based on the chelation of the transition metal involved in the lipid peroxidation reactions. The results clearly indicated that RCG-TiO_2-Ag films displayed an antioxidant capacity (Fig. 9a). The higher the TiO_2-Ag NPs content is, the higher the DPPH radical scavenging activity is. The highest activity (48%) was recorded with TiO_2-Ag NPs content of 4%. Similarly, Hajji, et al. (2019) reported that Ag nanoparticles incorporated into the chitosan matrix exhibit a dose-dependent DPPH radical-scavenging efficiency. On the other hand, all tested films present a dose dependence on iron chelating activity, as displayed in Fig 9b. The highest activity up to 63 % was recorded for 4% NPs-added films, while the control film exhibited the lowest activity (about 23%). In this context, Nakkala, Mata, Raja, Chandra,

and Sadras (2018) demonstrated that silver nanoparticles can accept or lose electrons forming stable compounds, resulting in the free radicals' quench. Hence, the elaborated RCG films supplemented by TiO_2-Ag NPs may act as an antioxidant agent, thanks to their amino and hydroxyl groups, which may perform as proton-donors.

Conclusion

In the present study, TiO_2-Ag NPs were successfully incorporated into a RCG matrix as nanosized fillers. The content of nanoparticles affected the microstructure as well as the mechanical properties and the thermal stability of the elaborated films. Interestingly, the thermal stability of the 3D polymeric matrix of RCG films was tightly related to the concentration of nanoparticles. Furthermore, the RCG films supplemented with the adequate TiO_2-Ag NPs content showed an improvement in their *in vitro* antioxidant activities, thermal stability as well as a gradual decrease in their EAB values leading to the amelioration of the nanocomposite films rigidity. Therefore, RCG/TiO_2-Ag NPs composite films could be promising for potential uses in water-soluble food packaging.

Acknowledgments

This research work was conducted in the framework of PHC-Utique Program, (partenariat Hubert Curien « Utique » du Ministère de l'Europe et des Affaires Etrangères français et du Ministère de l'Enseignement et de la Recherche Scientifique tunisien) financed by CMCU (Comité mixte de coopération universitaire), grant N°: 19G0815.

References

Abdelhedi, O., Jridi, M., Nasri, R., Mora, L., Toldrá, F., & Nasri, M. (2019). Rheological and structural properties of *Hemiramphus far* skin gelatin: Potential use as an active fish coating agent. *Food Hydrocolloids, 87,* 331-341.

Abdelhedi, O., Nasri, R., Souissi, N., Nasri, M., & Jridi, M. (2016). Sulfated polysaccharides from common smooth hound: Extraction and assessment of anti-ACE, antioxidant and antibacterial activities. *Carbohydrate Polymers, 152*, 605-614.

Ahmad, M., Benjakul, S., Prodpran, T., & Agustini, T. W. (2012). Physico-mechanical and antimicrobial properties of gelatin film from the skin of unicorn leatherjacket incorporated with essential oils. *Food Hydrocolloids, 28*(1), 189-199.

Alebooyeh, R., Mohammadi Nafchi, A., & Jokar, M. (2012). The Effects of ZnOnanorodson the Characteristics of Sago Starch Biodegradable Films. *Journal of Chemical Health Risks, 2*(4), 13-16.

Al-Hassan, A. (2020). Gelatin from camel skins: Extraction and characterizations. *Food Hydrocolloids, 101*, 105457.

Ali, A. M. M., Kishimura, H., & Benjakul, S. (2018). Physicochemical and molecular properties of gelatin from skin of golden carp (*Probarbus Jullieni*) as influenced by acid pretreatment and prior-ultrasonication. *Food Hydrocolloids, 82*, 164-172.

Arfat, Y. A., Benjakul, S., Prodpran, T., & Osako, K. (2014). Development and characterisation of blend films based on fish protein isolate and fish skin gelatin. *Food Hydrocolloids, 39*, 58-67.

Arfat, Y. A., Benjakul, S., Prodpran, T., Sumpavapol, P., & Songtipya, P. (2016). Physico-mechanical characterization and antimicrobial properties of fish protein isolate/fish skin

519 gelatin-zinc oxide (ZnO) nanocomposite films. *Food and Bioprocess Technology*, *9*(1),
520 101-112.
521 Arumugam, G. K. S., Sharma, D., Balakrishnan, R. M., & Ettiyappan, J. B. P. (2018).
522 Extraction, optimization and characterization of collagen from sole fish skin. *Sustainable*
523 *Chemistry and Pharmacy*, *9*, 19-26.
524 Ba-Abbad, M. M., Kadhum, A. A. H., Mohamad, A. B., Takriff, M. S., & Sopian, K. (2012).
525 Synthesis and catalytic activity of TiO_2 nanoparticles for photochemical oxidation of
526 concentrated chlorophenols under direct solar radiation. *International Journal*
527 *Electrochemestry Science*, *7*(6), 4871-4888.
528 Bahadur, K. R., & Uludağ, H. (2016). 2 - PEI and its derivatives for gene therapy. *Polymers*
529 *and Nanomaterials for Gene Therapy*. 29-54.
530 Bell, L. N., & Touma, D. E. (1996). Glass transition temperatures determined using a
531 temperature- cycling differential scanning calorimeter. *Journal of Food Science*, *61*(4),
532 807-810.
533 Bergo, P., Moraes, I. C. F., & Sobral, P. J. d. A. (2013). Effects of plasticizer concentration
534 and type on moisture content in gelatin films. *Food Hydrocolloids*, *32*(2), 412-415.
535 Bersuder, P., Hole, M., & Smith, G. (1998). Antioxidants from a heated histidine-glucose
536 model system. I: Investigation of the antioxidant role of histidine and isolation of
537 antioxidants by high-performance liquid chromatography. *Journal of the American Oil*
538 *Chemists' Society*, *75*(2), 181-187.
539 Chak, V., Kumar, D., & Visht, S. (2013). A review on collagen based drug delivery systems.
540 *International Journal of Pharmacy Teaching and Practices*, *4*(4), 811-820.
541 Chang, S.-T., Chen, L.-C., Lin, S.-B., & Chen, H.-H. (2012). Nano-biomaterials application:
542 Morphology and physical properties of bacterial cellulose/gelatin composites via
543 crosslinking. *Food Hydrocolloids*, *27*(1), 137-144.

Chen, I.-C., Hsiao, I.-L., Lin, H.-C., Wu, C.-H., Chuang, C.-Y., & Huang, Y.-J. (2016). Influence of silver and titanium dioxide nanoparticles on in vitro blood-brain barrier permeability. *Environmental toxicology and pharmacology, 47*, 108-118.

Chuaynukul, K., Prodpran, T., & Benjakul, S. (2014). Preparation, thermal properties and characteristics of gelatin molding compound resin. *Research Journal of Chemistry and Environment SCImago, 2*, 1-9.

De Moura, M., Avena- Bustillos, R., McHugh, T., Krochta, J., & Mattoso, L. (2008). Properties of novel hydroxypropyl methylcellulose films containing chitosan nanoparticles. *Journal of Food Science, 73*(7), 31-37.

de Moura, M. R., Lorevice, M. V., Mattoso, L. H., & Zucolotto, V. (2011). Highly stable, edible cellulose films incorporating chitosan nanoparticles. *Journal of Food Science, 76*(2), 25-29.

Decker, E. A., & Welch, B. (1990). Role of ferritin as a lipid oxidation catalyst in muscle food. *Journal of Agricultural and Food Chemistry, 38*(3), 674-677.

Decker, H., & Rimke, T. (1998). Tarantula hemocyanin shows phenoloxidase activity. *Journal of Biological Chemistry, 273*(40), 25889-25892.

Elleuch, L., Messaoud, M., Djebali, K., Attafi, M., Cherni, Y., Kasmi, M., Elaoud, A., Trabelsi, I., & Chatti, A. (2020). A new insight into highly contaminated landfill leachate treatment using Kefir grains pre-treatment combined with Ag-doped TiO2 photocatalytic process. *Journal of Hazardous Materials, 382*, 121119.

Félix, M., Lucio-Villegas, A., Romero, A., & Guerrero, A. (2016). Development of rice protein bio-based plastic materials processed by injection molding. *Industrial Crops and Products, 79*, 152-159.

Feng, X.-X., Zhang, L.-L., Chen, J.-Y., Guo, Y.-H., Zhang, H.-P., & Jia, C.-I. (2007). Preparation and characterization of novel nanocomposite films formed from silk fibroin and nano-TiO2. *International journal of biological macromolecules, 40*(2), 105-111.

Fernández-Díaz, M. D., Montero, P., & Gómez-Guillén, M. C. (2001). Gel properties of collagens from skins of cod (*Gadus morhua*) and hake (*Merluccius merluccius*) and their modification by the coenhancers magnesium sulphate, glycerol and transglutaminase. *Food Chemistry, 74*(2), 161-167.

Fundo, J. F., Galvis-Sanchez, A. C., Delgadillo, I., Silva, C. L. M., & Quintas, M. A. C. (2015). The effect of polymer/ plasticiser ratio in film forming solutions on the properties of chitosan films. *Food Biophysics, 10*(3), 324-333.

Galiano, F., Briceño, K., Marino, T., Molino, A., Christensen, K. V., & Figoli, A. (2018). Advances in biopolymer-based membrane preparation and applications. *Journal of Membrane Science,564*, 562-586.

Gennadios, A., Handa, A., Froning, G. W., Weller, C. L., & Hanna, M. A. (1998). Physical properties of egg white− dialdehyde starch films. *Journal of agricultural and food chemistry, 46*(4), 1297-1302.

Gómez-Guillén, M., Pérez-Mateos, M., Gómez-Estaca, J., López-Caballero, E., Giménez, B., & Montero, P. (2009). Fish gelatin: a renewable material for developing active biodegradable films. *Trends in Food Science & Technology, 20*(1), 3-16.

Hajji, S., Khedir, S. B., Hamza-Mnif, I., Hamdi, M., Jedidi, I., Kallel, R., Boufi, S., & Nasri, M. (2019). Biomedical potential of chitosan-silver nanoparticles with special reference to antioxidant, antibacterial, hemolytic and in vivo cutaneous wound healing effects. *Biochimica et Biophysica Acta (BBA)-General Subjects, 1863*(1), 241-254.

Hamdi, M., Hammami, A., Hajji, S., Jridi, M., Nasri, M., & Nasri, R. (2017). Chitin extraction from blue crab (*Portunus segnis*) and shrimp (*Penaeus kerathurus*) shells using

592 digestive alkaline proteases from *P. segnis* viscera. *International journal of biological*
593 *macromolecules, 101*, 455-463.
594 Hamzeh, A., Benjakul, S., Sae-leaw, T., & Sinthusamran, S. (2018). Effect of drying methods
595 on gelatin from splendid squid (*Loligo formosana*) skins. *Food Bioscience, 26*, 96-103.
596 Handbook, G. G. (2012). Gelatin Manufacturers Institute of America. *Inc., New York, NY*.
597 Haug, I. J., Draget, K. I., & Smidsrød, O. (2004). Physical and rheological properties of fish
598 gelatin compared to mammalian gelatin. *Food Hydrocolloids, 18*(2), 203-213.
599 Hazirah, M. N., Isa, M., & Sarbon, N. (2016). Effect of xanthan gum on the physical and
600 mechanical properties of gelatin-carboxymethyl cellulose film blends. *Food Packaging*
601 *and Shelf Life, 9*, 55-63.
602 Hosseini, S. F., Rezaei, M., Zandi, M., & Farahmandghavi, F. (2015). Fabrication of bio-
603 nanocomposite films based on fish gelatin reinforced with chitosan nanoparticles. *Food*
604 *Hydrocolloids, 44*(0), 172-182.
605 Jamróz, E., Kulawik, P., & Kopel, P. (2019). The effect of nanofillers on the functional
606 properties of biopolymer-based films: A review. *Polymers, 11*(4), 675.
607 Jridi, M., Nasri, R., Lassoued, I., Souissi, N., Mbarek, A., Barkia, A., & Nasri, M. (2013).
608 Chemical and biophysical properties of gelatins extracted from alkali-pretreated skin of
609 cuttlefish (*Sepia officinalis*) using pepsin. *Food Research International, 54*(2), 1680-1687.
610 Kamal, O., Pochat-Bohatier, C., & Sanchez-Marcano, J. (2017). Development and stability of
611 gelatin cross-linked membranes for copper (II) ions removal from acid waters. *Separation*
612 *and Purification Technology, 183*, 153-161.
613 Karayannakidis, P. D., & Zotos, A. (2016). Fish processing by-products as a potential source
614 of gelatin: a review. *Journal of Aquatic Food Product Technology, 25*(1), 65-92.

615 Karim, A. A., & Bhat, R. (2008). Gelatin alternatives for the food industry: recent
616 developments, challenges and prospects. *Trends in Food Science & Technology*, *19*(12),
617 644-656.
618 Kchaou, H., Jridi, M., Abdelhedi, O., Nasreddine, B., Karbowiak, T., Nasri, M., &
619 Debeaufort, F. (2017). Development and characterization of cuttlefish (*Sepia officinalis*)
620 skin gelatin-protein isolate blend films. *International journal of biological*
621 *macromolecules, 105*, 1491-1500.
622 Khan, I., Saeed, K., & Khan, I. (2019). Nanoparticles: Properties, applications and toxicities.
623 *Arabian Journal of Chemistry,12* (7), 908-931.
624 Laemmli, U. K. (1970). Cleavage of structural proteins during the assembly of the head of
625 bacteriophage T4. *Nature, 227*(5259), 680-685.
626 Lassoued, I., Jridi, M., Nasri, R., Dammak, A., Hajji, M., Nasri, M., & Barkia, A. (2014).
627 Characteristics and functional properties of gelatin from thornback ray skin obtained by
628 pepsin-aided process in comparison with commercial halal bovine gelatin. *Food*
629 *Hydrocolloids, 41*(0), 309-318.
630 Li, X., Xu, H., Chen, Z.-S., & Chen, G. (2011). Biosynthesis of nanoparticles by
631 microorganisms and their applications. *Journal of Nanomaterials*, *2011*.
632 Liu, H., Li, D., & Guo, S. (2008). Rheological properties of channel catfish (*Ictalurus*
633 *punctaus*) gelatine from fish skins preserved by different methods. *LWT - Food Science*
634 *and Technology, 41*(8), 1425-1430.
635 Luecha, J., Sozer, N., & Kokini, J. L. (2010). Synthesis and properties of corn
636 zein/montmorillonite nanocomposite films. *Journal of Materials Science, 45*(13), 3529-
637 3537.
638 Maccari, F., Galeotti, F., & Volpi, N. (2015). Isolation and structural characterization of
639 chondroitin sulfate from bony fishes. *Carbohydrate Polymers, 129*, 143-147.

640 Mangalaraj, D., & Devi, D. N. (2017). Ag/TiO_2 (Metal/Metal Oxide) Core Shell
641 Nanoparticles for Biological Applications. In *Recent Trends in Materials Science and*
642 *Applications* (pp. 9-17): Springer.
643 Minecka, A., Kamińska, E., Tarnacka, M., Jurkiewicz, K., Talik, A., Wolnica, K., Dulski, M.,
644 Kasprzycka, A., Spychalska, P., & Garbacz, G. (2020). Does the molecular mobility and
645 flexibility of the saccharide ring affect the glass-forming ability of naproxen in binary
646 mixtures? *European Journal of Pharmaceutical Sciences*, 105091.
647 Mishra, R., Majeed, A., & Banthia, A. (2011). Development and characterization of
648 pectin/gelatin hydrogel membranes for wound dressing. *International Journal of Plastics*
649 *Technology*, *15*(1), 82-95.
650 Muyonga, J. H., Cole, C. G. B., & Duodu, K. G. (2004). Extraction and physico-chemical
651 characterisation of Nile perch (*Lates niloticus*) skin and bone gelatin. *Food Hydrocolloids*,
652 *18*(4), 581-592.
653 Nagarajan, M., Benjakul, S., Prodpran, T., & Songtipya, P. (2012). Properties of film from
654 splendid squid (Loligo formosana) skin gelatin with various extraction temperatures.
655 *International Journal of Biological Macromolecules*, *51*(4), 489-496.
656 Nakkala, J. R., Mata, R., Raja, K., Chandra, V. K., & Sadras, S. R. (2018). Green synthesized
657 silver nanoparticles: Catalytic dye degradation, in vitro anticancer activity and in vivo
658 toxicity in rats. *Materials Science and Engineering: C*, *91*, 372-381.
659 Naoi, K., Ohko, Y., & Tatsuma, T. (2005). Switchable rewritability of Ag–TiO 2
660 nanocomposite films with multicolor photochromism. *Chemical Communications* (10),
661 1288-1290.
662 Nur Hanani, Z. A., Beatty, E., Roos, Y. H., Morris, M. A., & Kerry, J. P. (2013).
663 Development and characterization of biodegradable composite films based on gelatin
664 derived from beef, pork and fish sources. *Foods*, *2*(1), 1-17.

Pereda, M., Dufresne, A., Aranguren, M. I., & Marcovich, N. E. (2014). Polyelectrolyte films based on chitosan/olive oil and reinforced with cellulose nanocrystals. *Carbohydrate Polymers, 101*, 1018-1026.

Poppe, H. (1997). Some reflections on speed and efficiency of modern chromatographic methods. *Journal of Chromatography A, 778*(1-2), 3-21.

Qiao, L., Zhang, Y., Hu, W., Guo, J., Cao, W., Ding, Z., Guo, Z., Fan, A., Song, J., & Huang, J. (2017). Synthesis, structural characterization and quantum chemical calculations on 1-(isomeric methylbenzoyl)-3-(4-trifluoromethylphenyl) thioureas. *Journal of molecular Structure, 1141*, 309-321.

Raghunath, A., & Perumal, E. (2017). Metal oxide nanoparticles as antimicrobial agents: a promise for the future. *International Journal of Antimicrobial Agents, 49*(2), 137-152.

Rahman, M. S., Al-Saidi, G. S., & Guizani, N. (2008). Thermal characterisation of gelatin extracted from yellowfin tuna skin and commercial mammalian gelatin. *Food Chemistry, 108*(2), 472-481.

Rhim, J.-W., Hong, S.-I., Park, H.-M., & Ng, P. K. (2006). Preparation and characterization of chitosan-based nanocomposite films with antimicrobial activity. *Journal of Agricultural and Food Chemistry, 54*(16), 5814-5822.

Schrieber, R., & Gareis, H. (2007). *Gelatine handbook: theory and industrial practice*: John Wiley & Sons.

Schulz, J., Hohenberg, H., Pflücker, F., Gärtner, E., Will, T., Pfeiffer, S., Wepf, R., Wendel, V., Gers-Barlag, H., & Wittern, K.-P. (2002). Distribution of sunscreens on skin. *Advanced drug delivery reviews, 54*, 157-163.

Serrano-León, J. S., Bergamaschi, K. B., Yoshida, C. M., Saldaña, E., Selani, M. M., Rios-Mera, J. D., Alencar, S. M., & Contreras-Castillo, C. J. (2018). Chitosan active films

containing agro-industrial residue extracts for shelf life extension of chicken restructured product. *Food Research International, 108*, 93-100.

Shankar, S., & Rhim, J.-W. (2018). Preparation of sulfur nanoparticle-incorporated antimicrobial chitosan films. *Food Hydrocolloids, 82*, 116-123.

Sinthusamran, S., Benjakul, S., Hemar, Y., & Kishimura, H. (2018). Characteristics and properties of gelatin from seabass (*Lates calcarifer*) swim bladder: impact of extraction temperatures. *Waste and Biomass Valorization, 9*(2), 315-325.

Sperling, L. H. (2005). *Introduction to physical polymer science*: John Wiley & Sons.

Tayebi, L., Rasoulianboroujeni, M., Cui, Z., & Ye, H. (2018). 3D-printed thick structured gelatin membrane for engineering of heterogeneous tissues. *Materials Letters, 217*, 39-43.

Theerawitayaart, W., Prodpran, T., Benjakul, S., & Sookchoo, P. (2019). Properties of films from fish gelatin prepared by molecular modification and direct addition of oxidized linoleic acid. *Food Hydrocolloids, 88*, 291-300.

Tkaczewska, J., Morawska, M., Kulawik, P., & Zając, M. (2018). Characterization of carp (*Cyprinus carpio*) skin gelatin extracted using different pretreatments method. *Food Hydrocolloids, 81*, 169-179.

Tongnuanchan, P., Benjakul, S., & Prodpran, T. (2012). Properties and antioxidant activity of fish skin gelatin film incorporated with citrus essential oils. *Food Chemistry, 134*(3), 1571-1579.

Tümerkan, E. T. A., Cansu, Ü., Boran, G., Mac Regenstein, J., & Özoğul, F. (2019). Physiochemical and functional properties of gelatin obtained from tuna, frog and chicken skins. *Food Chemistry, 287*, 273-279.

Tunç, S., & Duman, O. (2010). Preparation and characterization of biodegradable methyl cellulose/montmorillonite nanocomposite films. *Applied Clay Science, 48*(3), 414-424.

713 Vejdan, A., Ojagh, S. M., Adeli, A., & Abdollahi, M. (2016). Effect of TiO_2 nanoparticles on
714 the physico-mechanical and ultraviolet light barrier properties of fish gelatin/agar bilayer
715 film. *LWT-Food Science and Technology, 71*, 88-95.
716 Voon, H. C., Bhat, R., Easa, A. M., Liong, M., & Karim, A. (2012). Effect of addition of
717 halloysite nanoclay and SiO_2 nanoparticles on barrier and mechanical properties of bovine
718 gelatin films. *Food and bioprocess technology*, *5*(5), 1766-1774.
719 Wu, X., Liu, Y., Wang, W., Han, Y., & Liu, A. (2017). Improved mechanical and thermal
720 properties of gelatin films using a nano inorganic filler. *Journal of Food Process*
721 *Engineering, 40*(3), 12469.
722 Yan, J., Estévez, M. C., Smith, J. E., Wang, K., He, X., Wang, L., & Tan, W. (2007). Dye-
723 doped nanoparticles for bioanalysis. *Nano today, 2*(3), 44-50.
724 Zheng, L., Yu, H., Wei, H., Xing, Q., Zou, Y., Zhou, Y., & Peng, J. (2018). Antioxidative
725 peptides of hydrolysate prepared from fish skin gelatin using ginger protease activate
726 antioxidant response element-mediated gene transcription in IPEC-J2 cells. *Journal of*
727 *Functional Foods, 51*, 104-112.
728 Zhou, J., Wang, S., & Gunasekaran, S. (2009). Preparation and characterization of whey
729 protein film incorporated with TiO_2 nanoparticles. *Journal of Food Science, 74*(7), 50-56.
730
731
732
733
734
735
736
737
738

739 **Table 1.** Moisture content (MC), solubility, the glass transition temperature and mechanical
740 properties (tensile strength and elongation at break) of gelatin-based films supplemented with
741 different ratios of TiO_2-Ag NPs

TiO_2-Ag %	**MC** (g moisture/100 g wet basis film)	**Solubility** (%)	**Tg** (°C)	**Tensile strength** (MPa)	**Elongation at break** (%)
0	49.3±1.0[a]	33.12±6.59[a]	59.52	7.1±0.50[a]	28.1±2.5[a]
1	26.5±0.8[e]	29.02±3.52[b]	51.77	5.9±0.1[b]	21.6±0.2[b]
2	28.4±0.9[c]	30.53±2.37[b]	52.19	5.4±0.4[b]	18.7±0.8[c]
3	27. 8±0.4[d]	32.28±0.37[b]	51.80	5.3±0.1[b]	18.7±1.8[c]
4	31.3±0.1[b]	26.57±0.91[c]	52.61	5.2±0.7[b]	16.0±1.8[d]

742 [a,b,c,d,e] Letters in the same column within different nanoparticles content indicate significant
743 differences ($p < 0.05$**)**

744

745

746

747

748

749

750

751

752

Table 2. Color parameters of *R. cemiculus* gelatin films incorporated with TiO_2-Ag nanoparticles

TiO_2-Ag %	L*	a*	b*	ΔE
0	96.34±0.09[a]	-0.04±0.01[e]	1.13±0.02[e]	-
1	95.84±0.49[c]	0.27±0.04[d]	2.14±0.03[d]	1.38±0.11[d]
2	96.11±0.06[b]	0.42±0.04[c]	2.69±0.09[c]	2.70±0.09[c]
3	95.09±0.95[d]	0.77±0.01[a]	3.81±0.11[b]	9.39±1.0[b]
4	94.09±0.57[e]	0.76±0.11[b]	4.16±0.37[a]	14.85±1.0[a]

[a,b,c,d,e] Letters in the same column within different nanoparticles content indicate significant differences ($p < 0.05$**)**

Figure captions:

Figure 1. SDS-PAGE profiles of *R. cemiculus skin* gelatins. SD: standard, RCG: *R. cemiculus* gelatin.

Figure 2. Absorbance spectrum of *R. cemiculus* gelatin as a function of pH variation.

Figure 3. Light transmittance of films from *R. cemiculus* skin gelatin containing 1%, 2%, 3% and 4% of TiO_2 doped Ag nanoparticles.

Figure 4. Fourier transform infrared spectra of *R. cemiculus* skin gelatin films supplemented with different amount of TiO_2-Ag NPs.

Figure 5. X-ray diffraction patterns of *R. cemiculus* gelatin films with different amounts of TiO_2-Ag nanoparticles.

Figure 6. TGA thermograms and its temperature derivatives for *R. cemiculus* skin gelatin (a) and *R. cemiculus* skin gelatin supplemented with TiO2-Ag films (b, c).

Figure 7. SEM micrographs of cross-section (A) and surfaces (B) of gelatin/TiO_2-Ag. nanoparticles films: 0% (A, B), 1% (A1, B1), 2% (A2, B2), 3% (A3, B3) and 4% (A4, B4).

Figure 8. AFM 3D images and corresponding roughness curves of RCG gelatin films with different amounts of TiO_2-Ag nanoparticles: 0 wt % (A), 1 wt % (B), 4 wt % (C) on the gelatin basis.

Figure 9. Antioxidant activities of *R. cemiculus* skin gelatin containing 1%, 2%, 3% and 4% of TiO_2 doped Ag nanoparticles.

Fig. 1

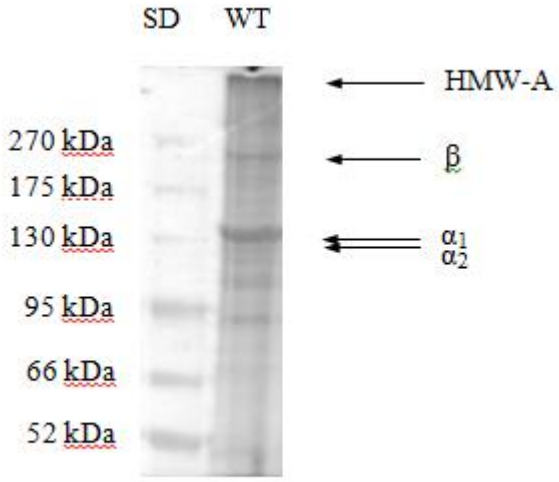

Fig. 2

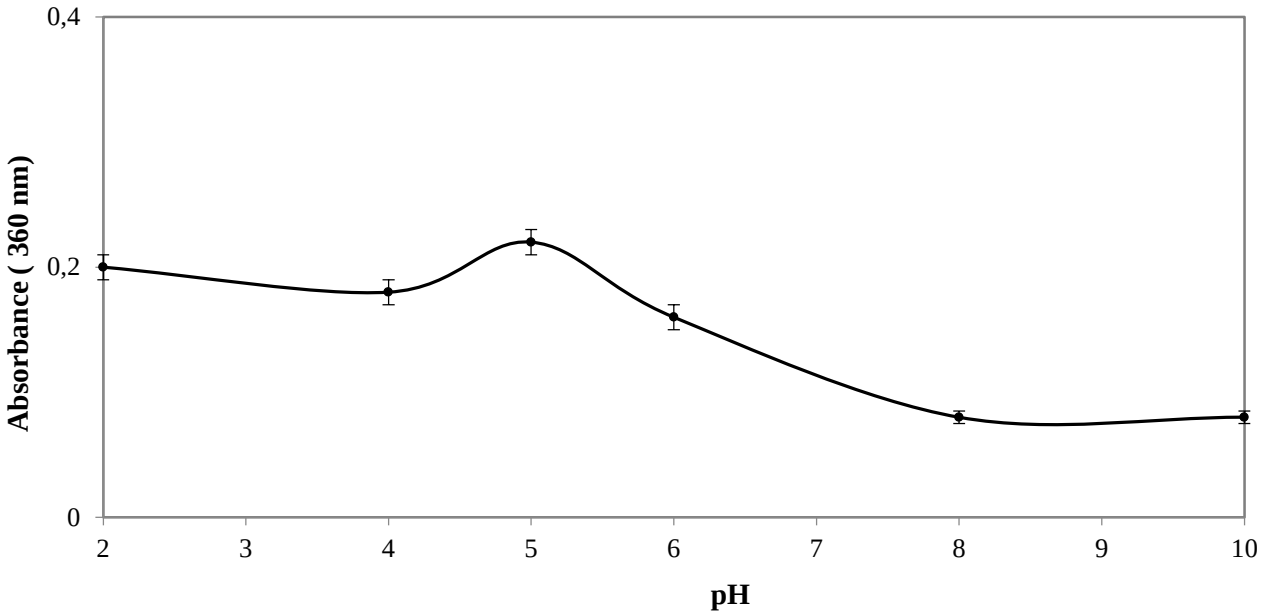

Fig. 3

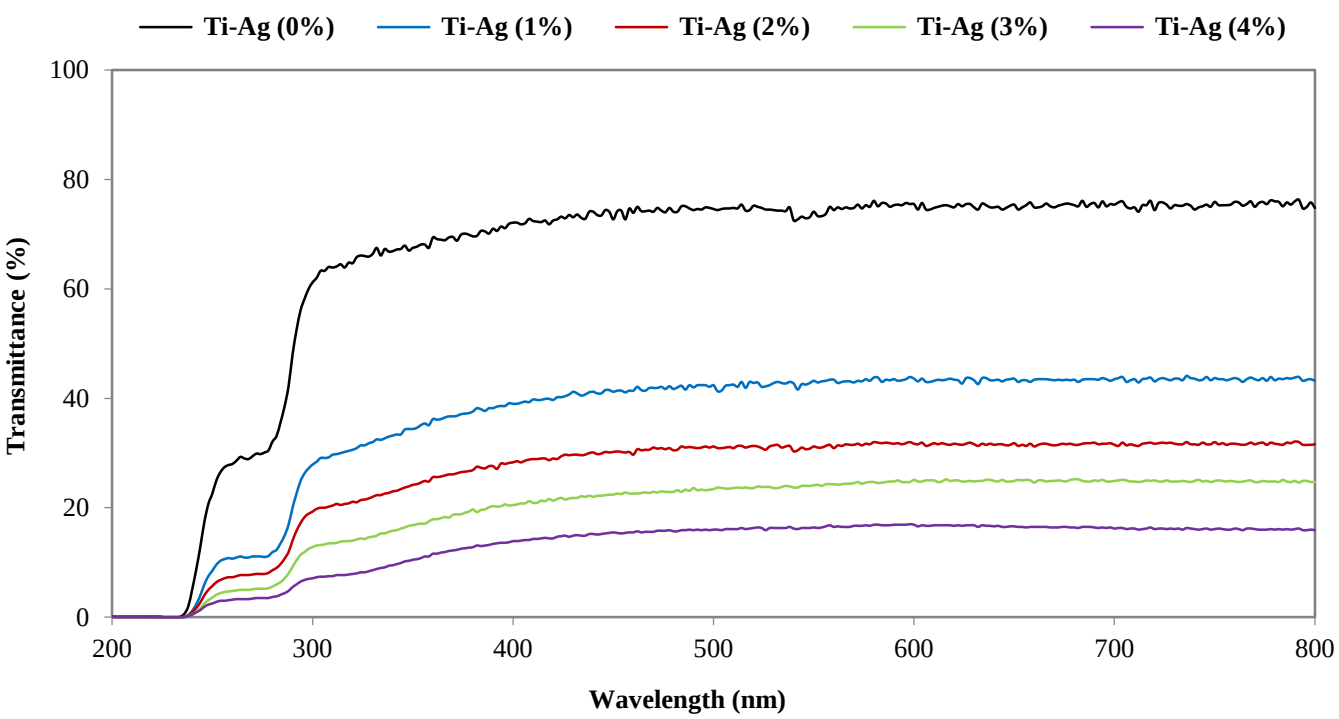
Ti-Ag (0%)
Ti-Ag (1%)
Ti-Ag (2%)
Ti-Ag (3%)
Ti-Ag (4%)
Transmittance (%)
100
80
60
40
20
0
200
300
400
500
600
700
800
Wavelength (nm)

Fig. 4

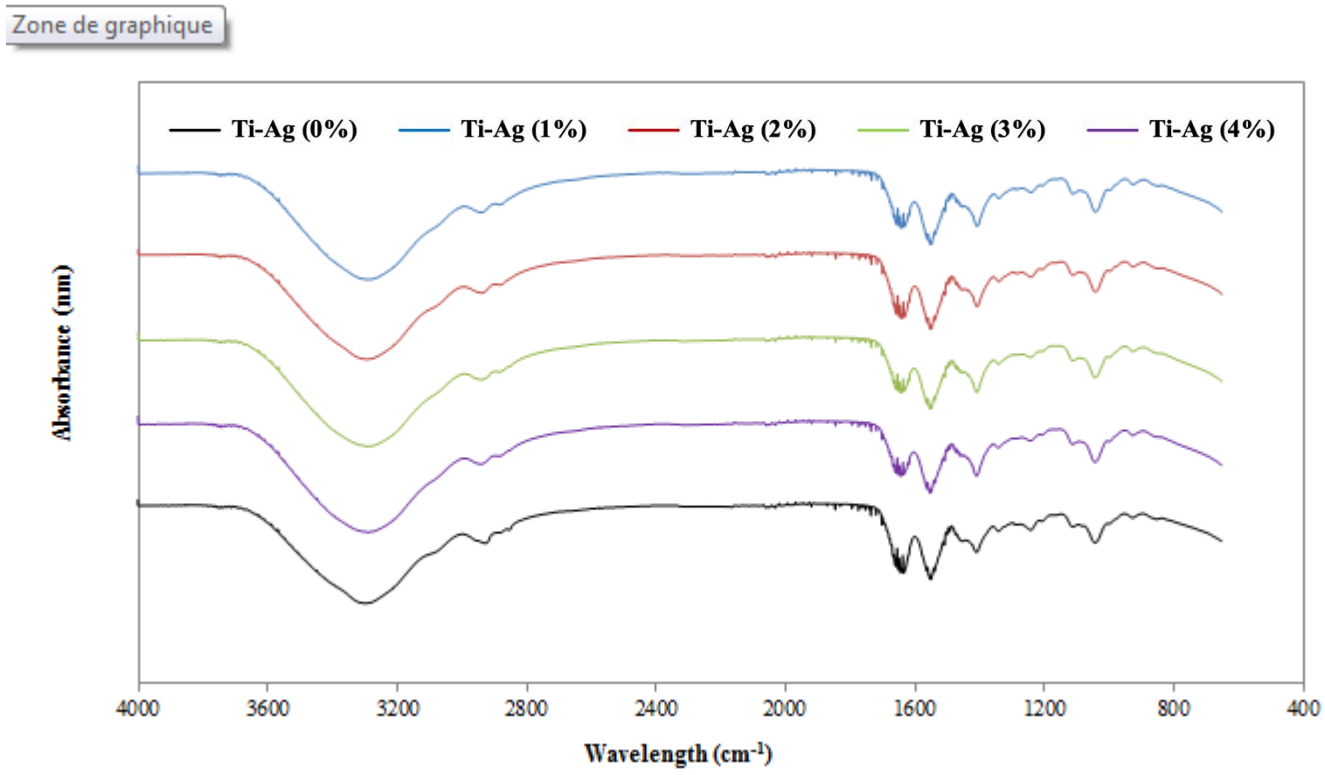
Zone de graphique
Ti-Ag (0%)
Ti-Ag (1%)
Ti-Ag (2%)
Ti-Ag (3%)
Ti-Ag (4%)
Absorbance (nm)
4000
3600
3200
2800
2400
2000
1600
1200
800
400
Wavelength (cm-1)

Fig. 5

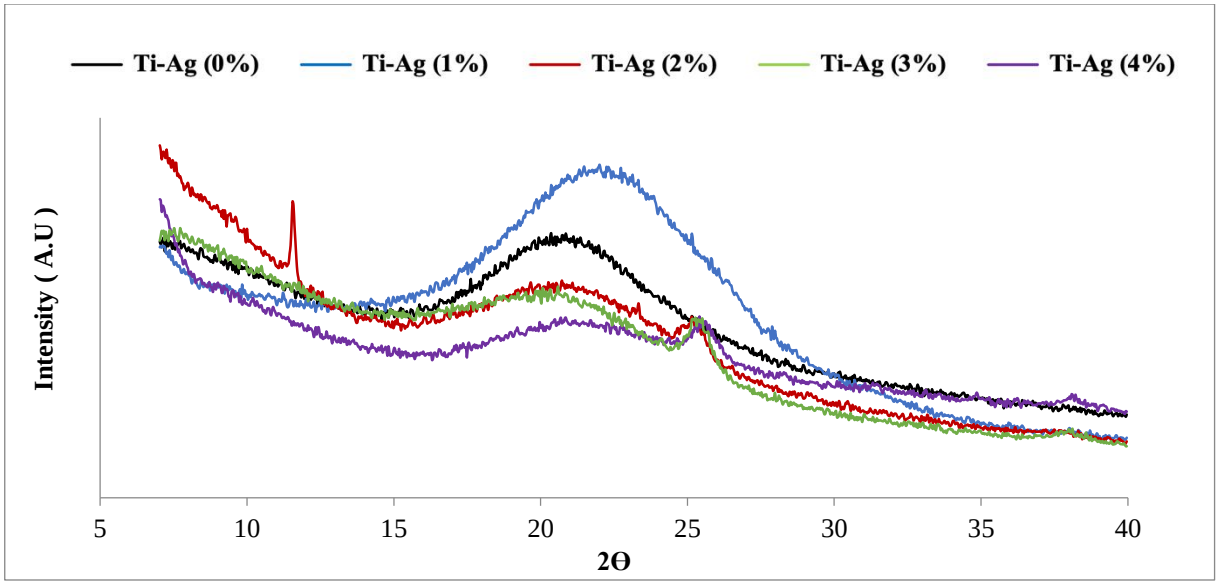
Ti-Ag (0%)
Ti-Ag (1%)
Ti-Ag (2%)
Ti-Ag (3%)
Ti-Ag (4%)
Intensity (A.U)
5
10
15
20
25
30
35
40
2Θ

Fig. 6

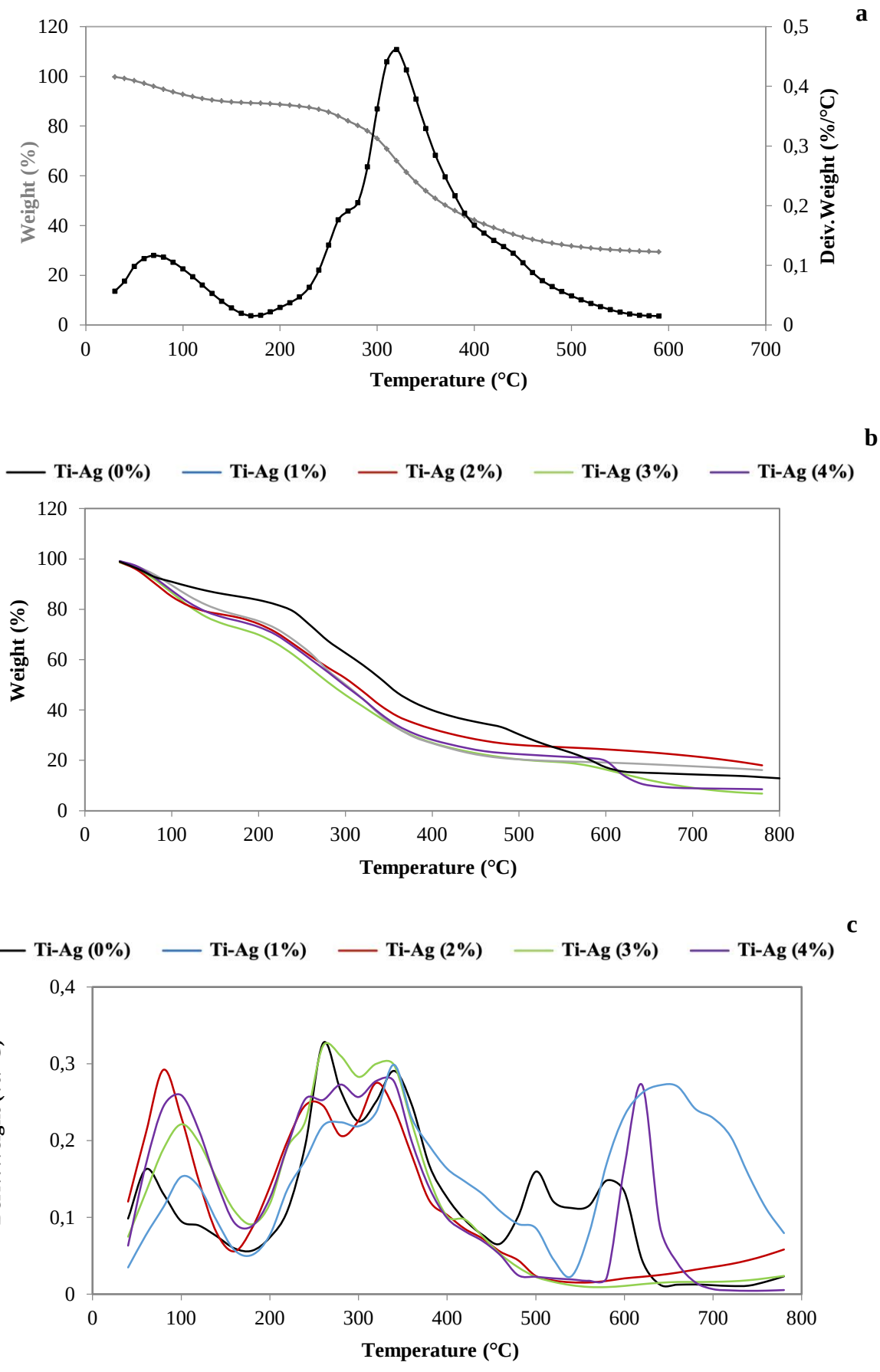
a
Weight (%)
Deiv.Weight (%/°C)
Temperature (°C)
b
Ti-Ag (0%)
Ti-Ag (1%)
Ti-Ag (2%)
Ti-Ag (3%)
Ti-Ag (4%)
Weight (%)
Temperature (°C)
c
Ti-Ag (0%)
Ti-Ag (1%)
Ti-Ag (2%)
Ti-Ag (3%)
Ti-Ag (4%)
Deriv.Weight (%/°C)
Temperature (°C)

Fig. 7

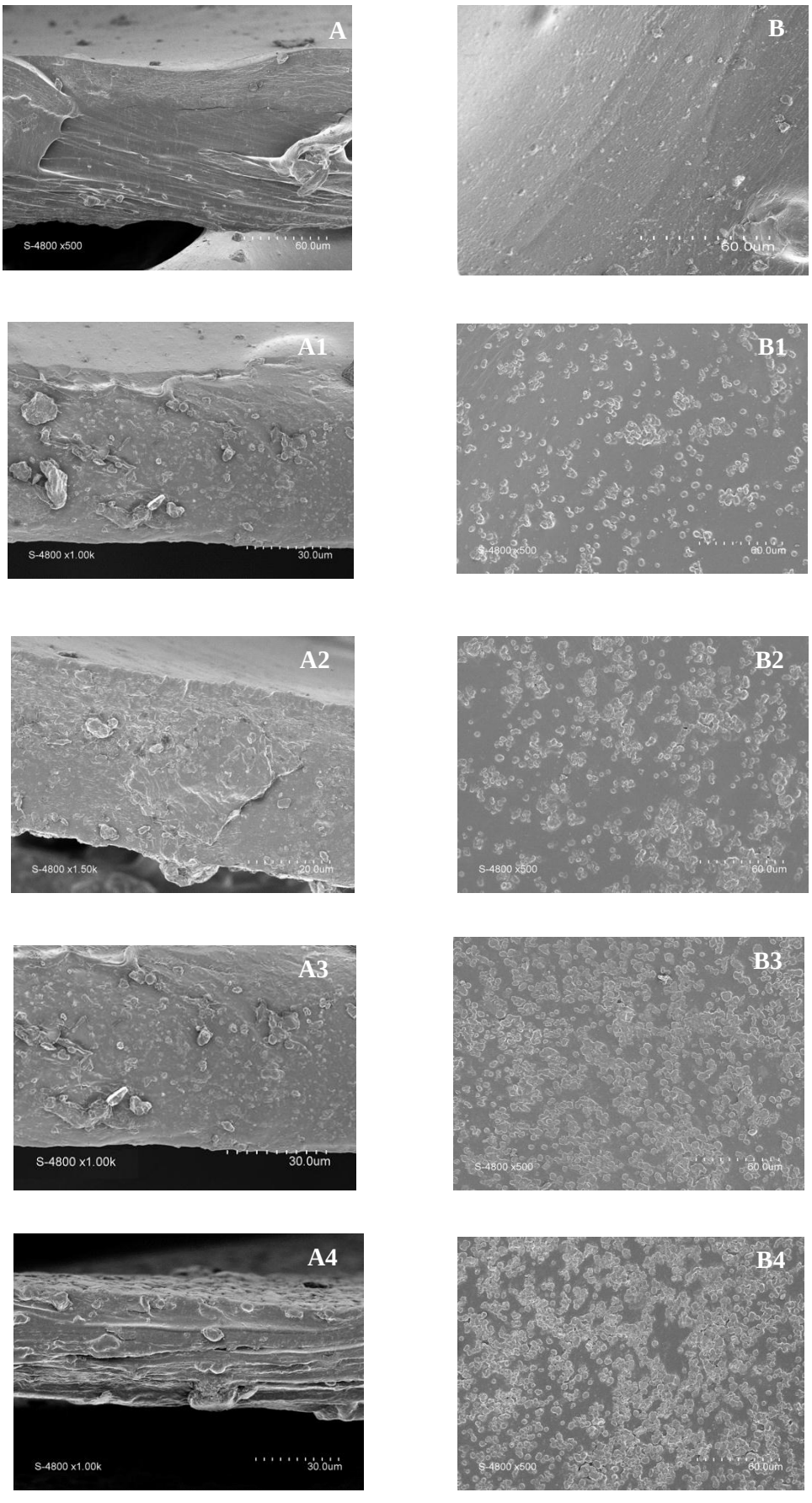
A
S-4800 x500
60.0um
B
60.0um
A1
S-4800 x1.00k
30.0um
B1
S-4800 x500
60.0um
A2
S-4800 x1.50k
20.0um
B2
S-4800 x500
60.0um
A3
S-4800 x1.00k
30.0um
B3
S-4800 x500
60.0um
A4
S-4800 x1.00k
30.0um
B4
S-4800 x500
60.0um

Fig. 8

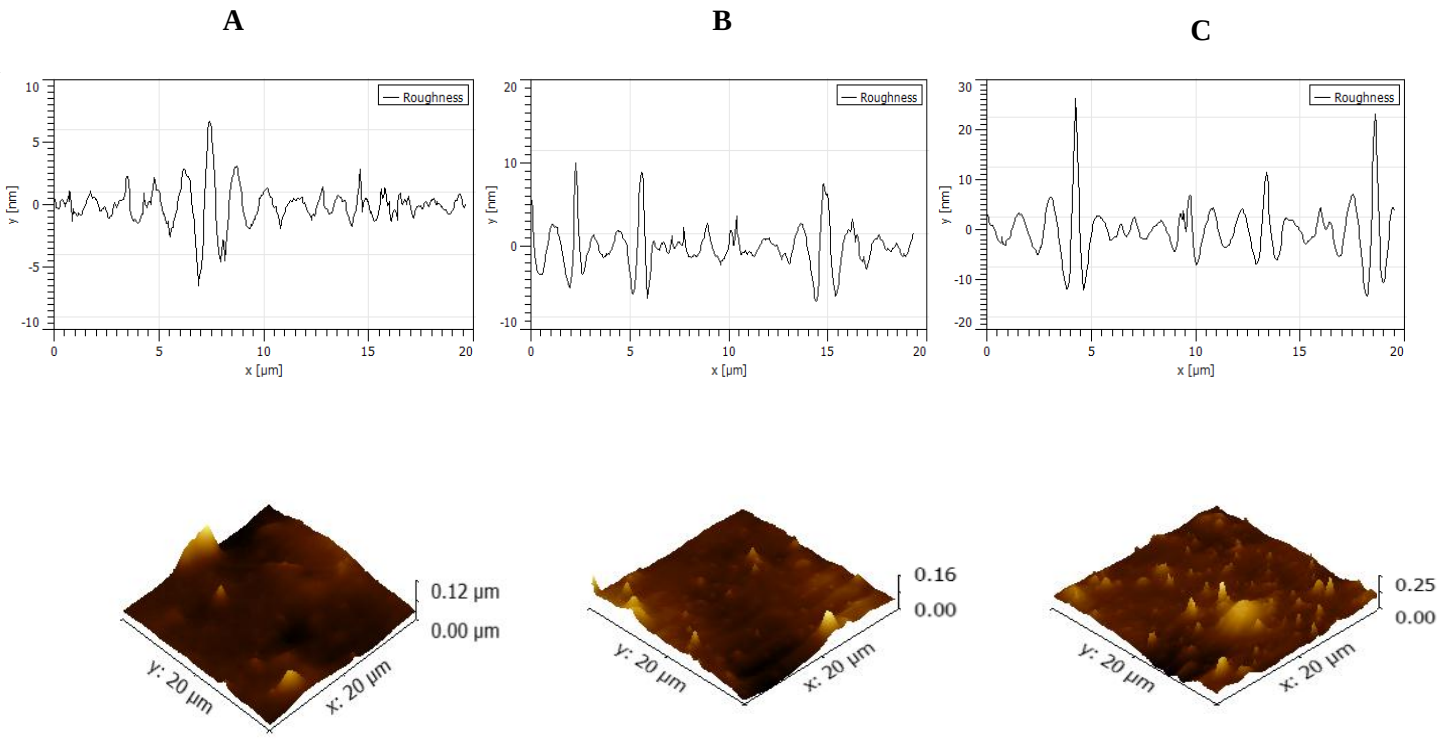
A
B
C
Roughness
y [nm]
x [µm]
0.12 µm
0.00 µm
0.16
0.00
0.25
0.00
y: 20 µm
x: 20 µm

Fig. 9

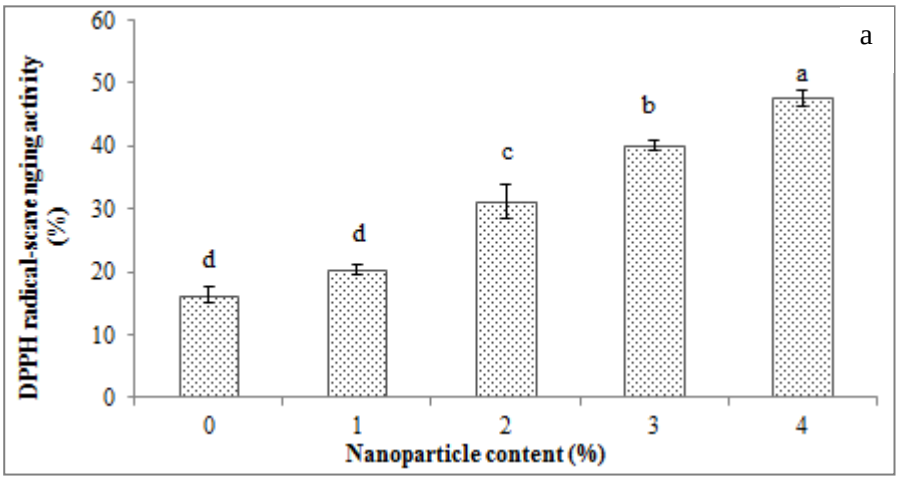
a
DPPH radical-scavenging activity (%)
60
50
40
30
20
10
0
d
d
c
b
a
0
1
2
3
4
Nanoparticle content (%)

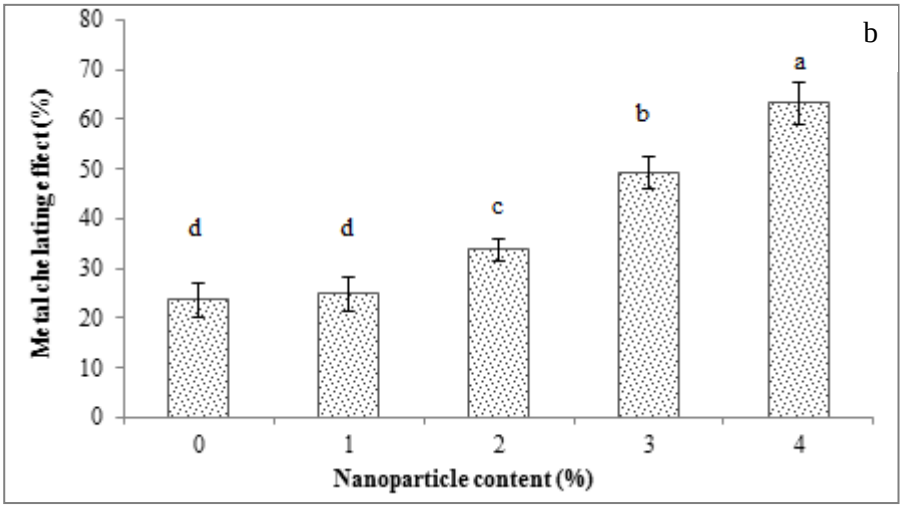
b
Metal chelating effect (%)
80
70
60
50
40
30
20
10
0
d
d
c
b
a
0
1
2
3
4
Nanoparticle content (%)